Plasmonics (2017) 12:1847–1853
DOI 10.1007/s11468-016-0453-5

A Highly Sensitive Dual-Core Photonic Crystal Fiber Based on a Surface Plasmon Resonance Biosensor with Silver-Graphene Layer

Famei Wang[1] · **Zhijie Sun**[1] · **Chao Liu**[2] · **Tao Sun**[3] · **Paul K. Chu**[4]

Received: 24 July 2016 / Accepted: 25 November 2016 / Published online: 17 December 2016

Abstract A highly sensitive dual-core photonic crystal fiber based on a surface plasmon resonance (PCF-SPR) biosensor with a silver-graphene layer is described. The silver layer with a graphene coating not only prevents oxidation of the silver layer but also can improve the silver sensing performance due to the large surface-to-volume ratio of graphene. The dual-core PCF-SPR biosensor is numerically analyzed by the finite-element method (FEM). An average spectral sensitivity of 4350 nm/refractive index unit (RIU) in the sensing range between 1.39 and 1.42 and maximum spectral sensitivity of 10,000 nm/RIU in the sensing range between 1.43 and 1.46 are obtained, corresponding to a high resolution of 1×10^{-6} RIU as a biosensor. Our analysis shows that the optical spectra of the PCF-SPR biosensor can be optimized by varying the structural parameters of the structure, suggesting promising applications in biological and biochemical detection.

Keywords PCF · SPR biosensor · Silver-graphene layer · FEM · Sensitivity

✉ Zhijie Sun
zhijiesun@hrbeu.edu.cn

✉ Chao Liu
msm-liu@126.com

[1] Institute of Materials Processing and Intelligent Manufacturing & Center for Biomedical Materials and Engineering, Harbin Engineering University, Harbin 150001, People's Republic of China

[2] School of Electronics Science, Northeast Petroleum University, Daqing 163318, People's Republic of China

[3] Institute of Microelectronics, Agency of Science, Technology and Research (A*STAR), Singapore 117685, Singapore

[4] Department of Physics and Materials Science, City University of Hong Kong, Tat Chee Avenue, Kowloon, Hong Kong, China

Introduction

Surface plasmon resonance (SPR) is a physical phenomenon in which a propagating evanescent electromagnetic wave is generated by oscillation of free electrons at a metal surface under the appropriate conditions [1]. Owing to the high sensitivity, sensing techniques based on SPR have recently undergone remarkable development in fields such as environmental monitoring, biotechnology, medical diagnostics, and food safety [2, 3]. In SPR-based sensors, the Kretschmann configuration is commonly used in which a thin metallic layer is deposited directly on a coupling prism [4]. However, the Kretschmann configuration is bulky and not suitable for remote and real-time sensing [5]. In order to overcome the limitation, SPR sensors with optical fibers have been proposed as they have advantages over prism-based SPR sensors, for instance, simple structure, small size, remote sensing capability, continuous analysis, and so on [6, 7]. In particular, SPR sensors with photonic crystal fiber (PCF) SPR, which have attracted much interest due to the flexibility in structural design, high sensitivity, and immunity to electromagnetic interference, have been numerically analyzed by the loss spectrum analysis method based on the coupled mode theory [8, 9].

In recent years, much effort has been devoted to the design of PCF-SPR biosensors because of applications such as analysis of biomolecular interactions (BIA) and detection of chemical and biological analytes [10–13]. Hassani et al. [14–16] proposed SPR sensors with two different structures based on PCF, analyzed the design principles with metallic coatings in biosensing applications, and achieved a refractive index resolution of 10^{-4} refractive index unit (RIU). X. Yu et al. [17] described a PCF-SPR in which a gold layer was coated onto the micro-channels of the sensor. Rifat et al. [18] proposed a simple liquid core PCF plasmonic biosensor with selectively filled analyte channels and observed enhanced

coupling between the surface plasmon polariton (SPP) mode and core-guided mode. This sensor showed a maximum spectral sensitivity of about 3000 nm/RIU in the refractive index sensing range between 1.46 and 1.49 corresponding to a resolution as high as 2.4×10^{-5} RIU.

In this study, we describe and numerically analyze a dual-core PCF-SPR biosensor with a silver-graphene layer as the sensitive materials. The resonance peak of silver is very sharp and may offer higher detection accuracy than gold. However, silver is chemically unstable under ambient conditions. In order to prevent oxidation and corrosion of silver and increase the surface-to-volume ratio, a graphene coating is introduced. Our analysis shows an average sensitivity of 4350 nm/RIU in the sensing range from 1.39 to 1.42, maximum spectral sensitivity of 10,000 nm/RIU from 1.43 to 1.46, as well as high linearity, corresponding to a high resolution of 1×10^{-6} RIU.

Geometry of a Dual-Core PCF-SPR Biosensor

The cross section of the proposed dual-core PCF-SPR biosensor is depicted in Fig. 1. The biosensor consists of two layers of air holes with different sizes arranged in an alternate way, and the central analyte channels are coated with a silver-graphene sensing layer. This structure couples the core-guided mode and plasmonic mode at the interface of silver-graphene and the analyte. The thickness of the silver and graphene layer is set as t_{Ag} = 40 nm and t_g = 4 nm, respectively. The dielectric constant of silver in the visible and near-IR region is defined by the Drude model [19]:

$$\varepsilon_{Ag}(\omega) = \varepsilon_\infty - \frac{\omega_p^2}{\omega(\omega + i\omega_\tau)} \tag{1}$$

where $\varepsilon_\infty = 9.84$, $\omega_p = 1.36 \times 10^{16}$, and $\omega_\tau = 1.018 \times 10^{14}$. The complex refractive index of graphene is described by the following equation [10]:

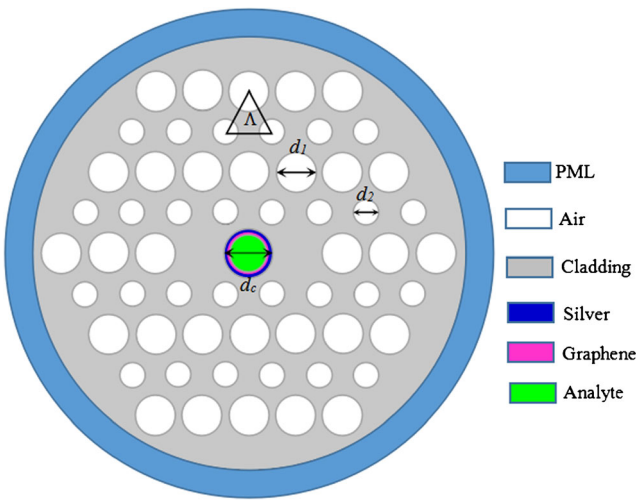

Fig. 1 Cross section of the dual-core PCF-SPR biosensor

$$n_g = 3 + iC_1\lambda/3 \tag{2}$$

The pitch size of the cladding air hole is $\Lambda = 2$ μm, the diameter of the small air holes is $d_2 = 0.5\Lambda$, and the diameter of the central analyte channel and large air holes is $d_c = d_1 = 0.8\Lambda$. The refractive index (n_c) of the analyte flowing through the channel ranges from 1.39 to 1.46, and n_a = 1.0 is the refractive index of the air. The refractive index of silica glass is given by the Sellmeier dispersion relation [20].

$$n^2 - 1 = \frac{0.6961663\lambda^2}{\lambda^2 - (0.0684043)^2} + \frac{0.4079426\lambda^2}{\lambda^2 - (0.1162414)^2} + \frac{0.897479\lambda^2}{\lambda^2 - (9.896161)^2} \tag{3}$$

The propagation loss is proportional to the imaginary part of the effective index and can be expressed as [21]

$$\alpha_{loss} = 40\pi \cdot \mathrm{Im}(n_{eff})/(\ln(10)\lambda) \approx 8.686 \times k_0 \cdot \mathrm{Im}(n_{eff})(dB/m) \tag{4}$$

where $n_{eff} = \beta/k_0$ is the effective index of the guide mode, λ is the free-space wavelength, and $k_0 = 2\pi/\lambda$ is the vacuum wavenumber. Excitation of surface plasmon can be characterized by calculating the loss of the optical fiber.

Analysis and Discussion

In this work, we use the 2D simulation mode analysis and the electromagnetic mode of the biosensor is solved by the finite-element method (FEM) using COMSOL Multiphysics software [19]. When the propagation loss of the core mode is utilized to evaluate the biosensing properties, a perfectly matched layer (PML) boundary condition is considered at numerical calculation zone edges [22]. Figure 2 shows the optical field distribution of the fundamental modes: (a) even mode for *x*-polarization, (b) odd mode for *x*-polarization, (c) even mode for *y*-polarization, and (d) odd mode for *y*-polarization, and the arrows represent the direction of the electric field. In the dual-core PCF-SPR biosensor, the even mode and odd mode for *x*-polarization and *y*-polarization are excited at the same time when energy goes into the fiber core. The total mode field can be regarded as a superposition of the even mode and odd mode for the two polarization directions. Most of the energy is gathered in the dual core by the cladding air holes, and only a fraction of the energy penetrates the silver-graphene-coated channel to excite the plasmon mode. The internal and external silver-graphene-coated surface can excite the plasmon mode, and the plasmon mode excited by the internal surface is more intense. Therefore, excitation of the plasmon mode on the metal surface is more intense in the low-refractive-index interface than in the high-refractive-index interface. Excitation of the plasmon mode is related to

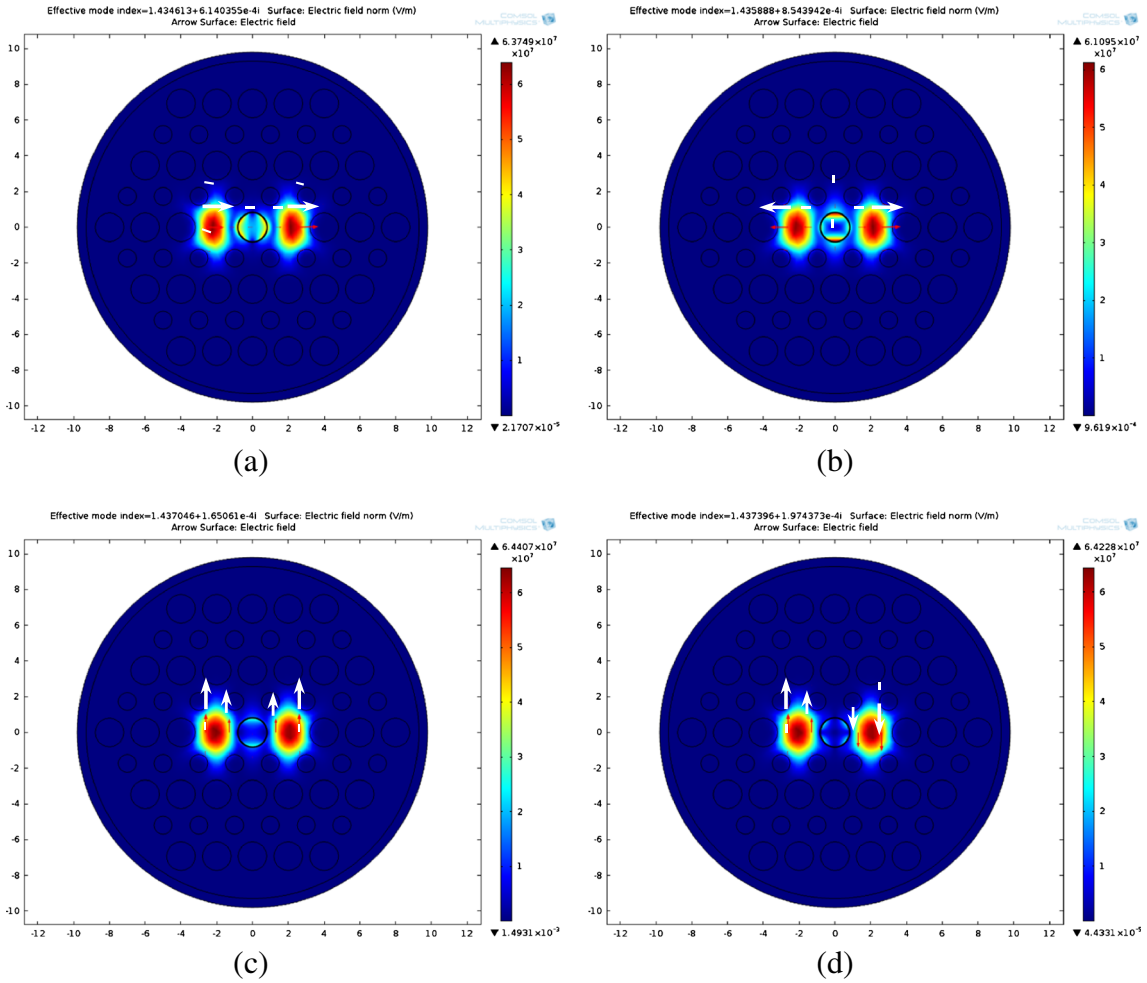

Fig. 2 Optical field distribution of the fundamental modes: **a** even mode for *x*-polarization, **b** odd mode for *x*-polarization, **c** even mode for *y*-polarization, and **d** odd mode for *y*-polarization

the change in the refractive index of the adjacent analyte. In the following numerical analysis, we focus on the even mode for *y*-polarization to evaluate the performance of the dual-core PCF-SPR biosensor.

Figure 3 shows the distribution of the refractive index of the biosensor. The blue line represents the propagation loss of the fundamental mode effective index, the black line represents the real part of the fundamental mode effective index, and the green line represents the dispersion relations of the surface plasmon mode. The imaginary part of the refractive index shows a sharp peak when the incident wavelength is 860 nm. The real part of the mode effective refractive index in the plural form shows the concept of the refractive index in the usual sense, and the imaginary part describes the mode loss. An obvious electromagnetic field overlap between the fundamental mode and surface plasmon mode is observed, and the phase matching coupling phenomenon is confirmed by the coincidence of the loss peak and intersection between the dispersion relations of the fundamental mode and surface plasmon mode as shown by point (*m*) in Fig. 3. Inset (a) displays the electric field distributions of the plasmonic mode, and light is confined on the surface of the silver-graphene-coated channel. Inset (b) presents the electric field distributions of the fundamental mode, and light is confined all to the dual core outside the resonant wavelength. Most of the energy is confined to the dual core, and only a part of the energy penetrates the silver-graphene-coated channel to the plasmon mode, as shown in inset (c) in Fig. 3. The energy loss of the core-guided mode is mainly because excitation generates the surface plasmon mode illustrating that the core-guided mode and plasma mode produce a resonance at 860 nm. The biosensor presents a plurality of formats because of the different propagation constants. The modes transferred to the core of the fiber are likely to meet the phase-matching condition and produce class surface plasma oscillations. Therefore, the resonance wavelengths of different modes are different [23].

The thickness of the metal film is the most important factor that affects the half width and amplitude of the resonant peak. The influence of different silver layer thicknesses on the biosensor performance is systemically investigated. The

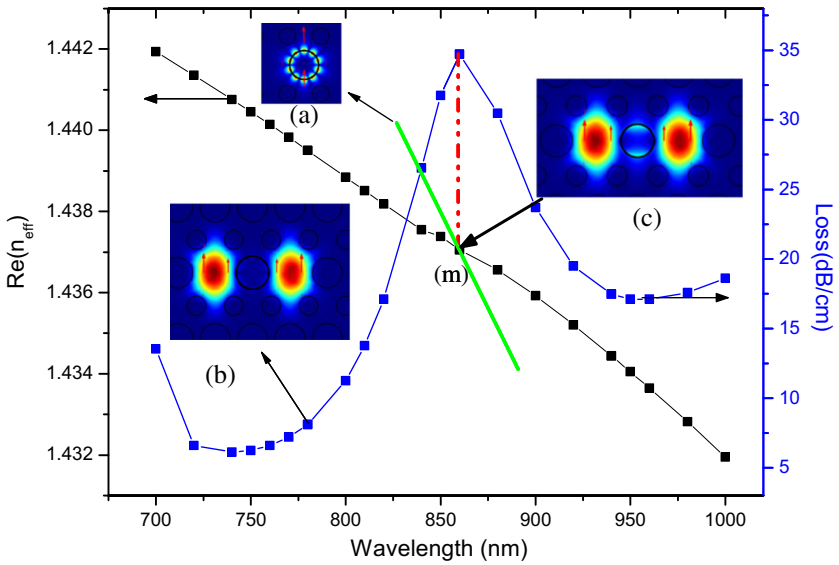

Fig. 3 Dispersion relation of the plasmonic mode (*green*), fundamental mode (*black*), and loss spectrum (*blue*) with *insets (a)*, *(b)*, and *(c)* showing the electric field distributions at each point

simulation results for the propagation loss of the fundamental mode for different silver layer thicknesses are shown in Fig. 4. The resonance wavelength moves towards a longer wavelength, and the intensity of the resonance peaks decreases gradually with increasing film thicknesses from 30 to 50 nm. Since the silver layer is coated on the surface of the center core, it means that more core energy is transferred to the SPW energy leading to stronger coupling efficiency. The increase in the overall effective index of the waveguide shifts the resonance to a longer wavelength. In addition, the resonance depth decreases while the half width of the resonant peak and loss at the off-resonance wavelength increase with increasing silver layer thicknesses throughout the calculated thickness range.

Figure 5 presents the loss spectra of the core mode for different core sizes. The resonance peak shifts to a longer wavelength, and the resonance depth increases for r_c between 0.75 and 0.85 when all the other structural parameters are kept constant. An increase in the propagation loss of the core-guided mode can be observed for a larger central hole. It can be explained by the fact that a larger hole in the center makes the metallic surface closer to the mode field. Therefore, the contact area between the mode field and metallic surface increased and more light is in turn coupled to the metallic surface, thus introducing more propagation losses. The increase in r_c also leads to a red shift in the resonance wavelength.

The fundamental mode loss spectra for different analytes are shown in Fig. 6a. The resonance peak shifts to a longer wavelength when the analyte refractive index is between 1.39 and 1.42. The resonance peak and depth increase gradually as the refractive index of the analyte increases. Since absorption by the silver layer depends on the refractive index of the ambient medium, the shift in the absorption wavelength can be detected even when the change in the refractive index of the analyte is very small [22]. Sensitivity can be enhanced by utilizing the refractive index of the analyte [20], and we

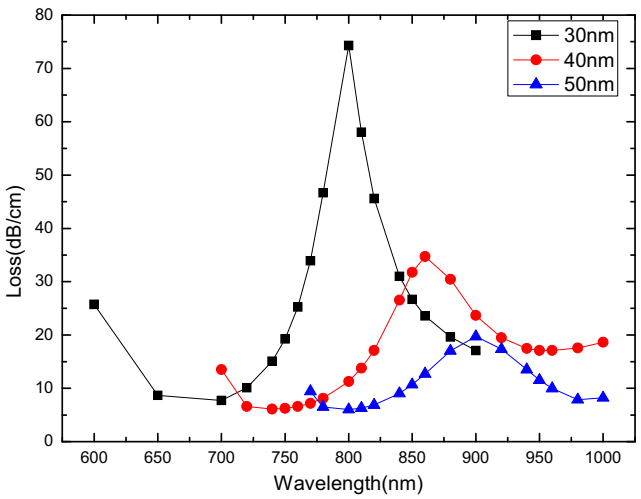

Fig. 4 Changes in the loss spectra of the plasmon peaks when the biosensor is coated with silver layers with different thicknesses

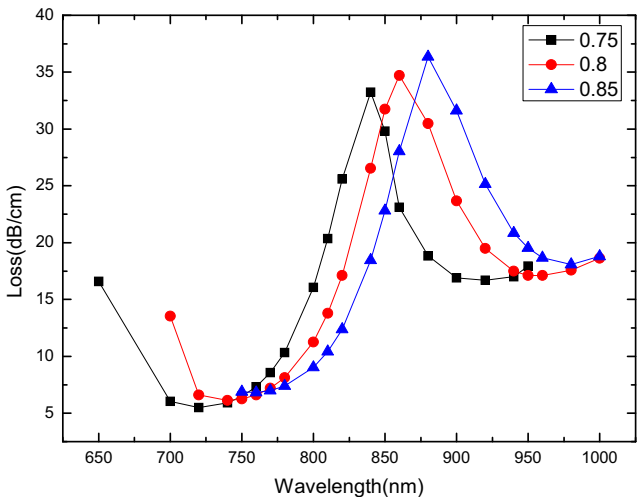

Fig. 5 Loss spectra of the fundamental mode for different sizes of core r_c

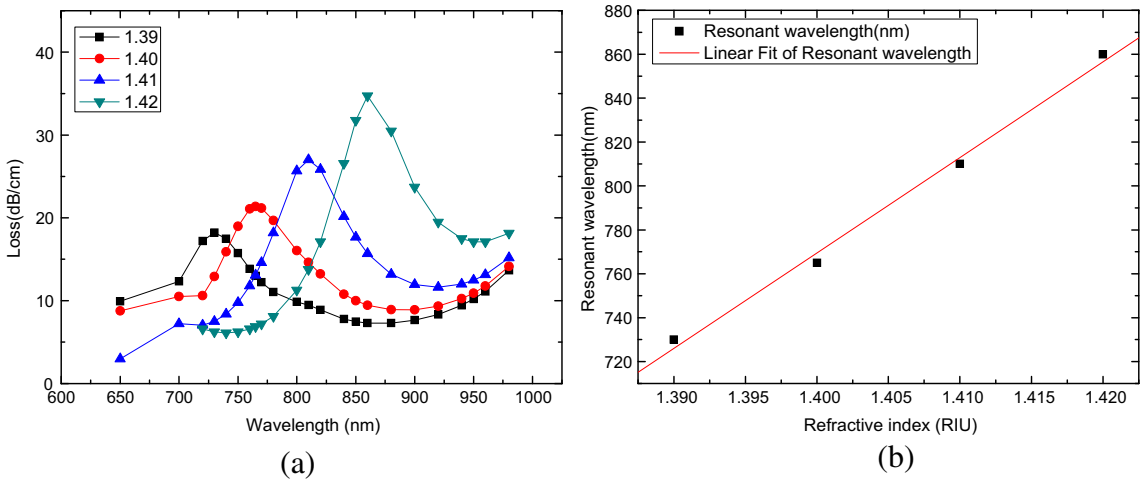

Fig. 6 **a** Loss spectra of the fundamental mode for the biosensor for different analytes and **b** linear fitting lines of the fundamental mode resonance wavelength versus analyte RI between 1.39 and 1.42

investigate the sensitivity of the PCF-SPR biosensor in the refractive index range of 1.39–1.42. The corresponding linear fitting curve of the resonance wavelength in relation to the refractive index of the analyte is presented in Fig. 6b. The fitting formula can be expressed by

$$\lambda\ (\mathrm{nm}) = 4350n - 5320.5,\ 1.39 \le n_a \le 1.42 \tag{5}$$

where λ is the resonance wavelength of the biosensor and n is the refractive index of the analyte. The slope of the equation reveals an average sensitivity of 4350 nm/RIU in the relevant sensing range. The adjusted R-square value of λ is 0.99698 indicating high linearity. The wavelength resolution of the detector is assumed to be $\Delta\lambda_{\min} = 0.1$ nm, and the refractive index resolution of the biosensor can be defined as [24]

$$R = \Delta n_a \Delta\lambda_{\min} / \Delta\lambda_{\mathrm{peak}} \tag{6}$$

Hence, the peak shift here is estimated to be about $\Delta\lambda_{\mathrm{peak}} = 50$ nm according to Fig. 6a. When the variation in the analyte refractive index is $\Delta n_a = 0.01$, the sensitivity of the PCF-SPR biosensor is approximately 4350 nm/RIU for refractive indexes between 1.39 and 1.42, giving rise to a resolution of 2×10^{-6} RIU.

The fundamental mode loss spectra for different analytes are shown in Fig. 7a. The resonance peak shifts to a longer wavelength when the analyte refractive index is between 1.43 and 1.46. The resonance peak and depth increase gradually as the refractive index of the analyte increases. We investigate the sensitivity of the PCF-SPR biosensor in the analyte refractive index range of 1.43 to 1.46, and the corresponding linear fitting curve of the resonance wavelength in relation to the refractive index is presented in Fig. 7b. The fitting formula can be expressed by

$$\lambda\ (\mathrm{nm}) = 9200n - 12214,\ 1.43 \le n_a \le 1.46 \tag{7}$$

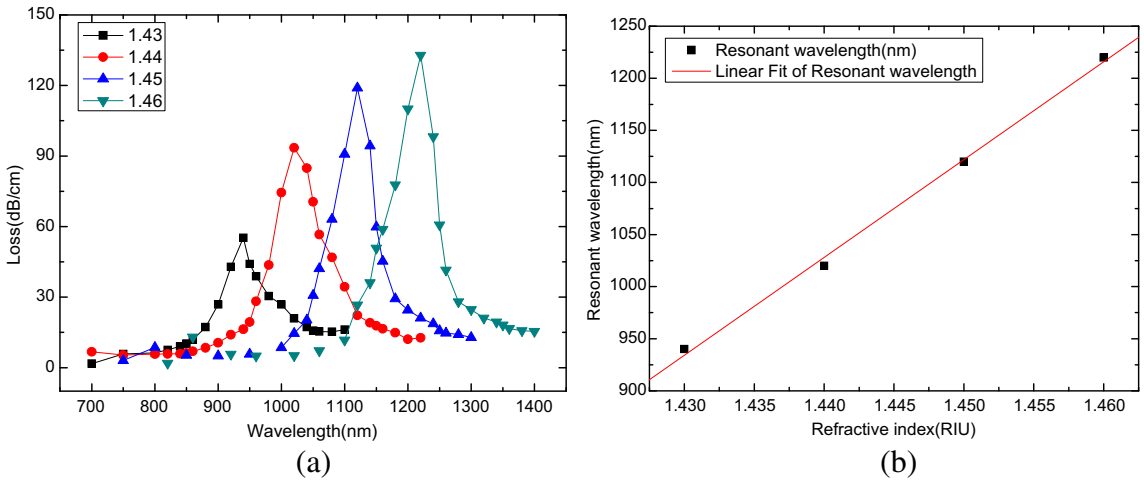

Fig. 7 **a** Loss spectra of the fundamental mode for the biosensor for different analytes and **b** linear fitting lines of the fundamental mode resonance wavelength versus analyte RI between 1.43 and 1.46

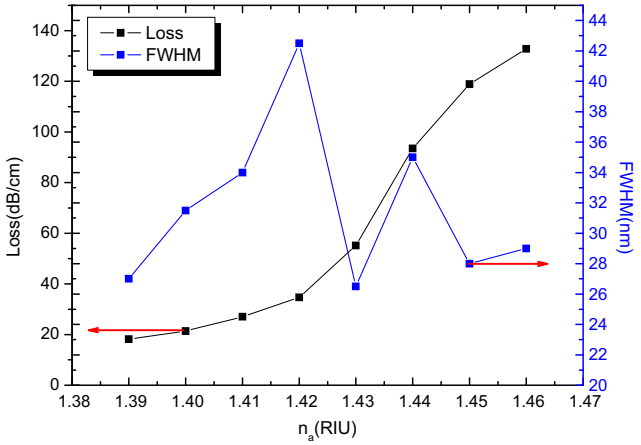

Fig. 8 Peak loss (*black*) of the fundamental mode for the dual-core PCF-SPR biosensor and FWHM (*blue*) on the analyte RI

where λ is the resonance wavelength of the biosensor and n is the refractive index of the analyte. The slope of the equation reveals an average sensitivity of 9200 nm/RIU in the relevant sensing range. The adjusted R-square value of λ is 0.99864 indicating high linearity. In the wavelength interrogation mode, variations in the refractive index of the analyte can be obtained by measuring the spectral peak displacement and the spectral sensitivity S is expressed as [25]

$$S(\lambda) = \frac{\Delta\lambda_{\text{peak}}}{\Delta n_{\text{a}}}(\text{nm/RIU}) \tag{8}$$

The peak shift in this work is estimated to be about $\Delta\lambda_{\text{peak}} = 100$ nm according to Fig. 7a. The wavelength resolution of the detector is assumed to be $\Delta\lambda_{\text{min}} = 0.1$ nm. When the variation in the analyte refractive index is $\Delta n_{\text{a}} = 0.01$, the maximum spectral sensitivity of the PCF-SPR biosensor is 10,000 nm/RIU for refractive indexes between 1.43 and 1.46 resulting in a resolution of 1×10^{-6} RIU.

Besides the sensitivity, dynamic operation range, linearity, and resolution, the full width at half maxima (FWHM) is a crucial parameter of a biosensor [26]. In a practical SPR sensing system, a smaller FWHM is favorable as the spectral noise is filtered more effectively [27, 28]. The FWHM results in not only smaller spectral deviation from the actual center of the resonant wavelength but also suppression of the non-resonance propagation loss [29]. The FWHM and resonant mode loss in the sensing range of 1.39–1.46 are presented in Fig. 8. The minimum FWHM is only 26.5 nm for $n_{\text{a}} = 1.43$. The resonant losses of the fundamental mode and SPP mode vary contrarily with an increasing analyte refractive index, and finally, they coincide with each other [30].

The proposed dual-core PCF-SPR biosensor here exhibits a great sensitivity to the refractive index of the surrounding medium. For the same refractive index dynamic detection ranges of 1.39–1.42 and 1.43–1.46, our dual-core PCF-SPR biosensor possesses spectral sensitivity values of 4350 and 10,000 nm/RIU higher than 2929.39 and 9231.27 nm/RIU described in ref. [20]. This maximum sensitivity value of 10,000 nm/RIU is an order of magnitude higher than 1000, 3000, and 4600 nm/RIU reported in refs. [18, 3231-]. Furthermore, the proposed biosensor in this work displays prominent characteristics of the higher resolution of 1×10^{-6} RIU, which is better than the resolution of 1×10^{-4} RIU and 3.03×10^{-5} RIU reported in [8, 21]. Based on the comparisons, it can be concluded that the sensing performance of the SPR sensors is enhanced by optimizing the dual-core PCF structure. The stronger power transfer between the two fiber cores is enhanced by the resonant coupling between the surface plasmon modes and the fiber core-guided modes.

Conclusion

A dual-core PCF-SPR biosensor with a silver-graphene sensing layer is described and analyzed. The silver layer with a graphene coating not only prevents oxidation of silver but also can improve the silver sensing performance due to a large surface-to-volume ratio. The coupling properties and sensing performance are numerically simulated by the finite-element method (FEM). The core-guided mode effective index and surface plasma mode are sensitive to the refractive index of the analyte. An average sensitivity of 4350 nm/RIU in the sensing range between 1.39 and 1.42, a maximum spectral sensitivity of 10,000 nm/RIU in the sensing range from 1.43 to 1.46, high linearity, and a high resolution of 1×10^{-6} RIU are achieved. On account of the promising results and simple sensing scheme, the biosensor has many potential applications in biological and biochemical sensing.

Acknowledgments This work was jointly supported by the National Natural Science Foundation of China (Grant No. 51474069), China Postdoctoral Science Foundation-funded project (Grant No. 2016 M59150), Natural Science Foundation of Heilongjiang Province (Grant No. E2016007), and City University of Hong Kong Applied Research Grant (ARG) No. 9667122.

References

1. Liu J, Chen B, Yang H, Mamoru I (2012) Symmetric surface plasmon resonance sensing structure excited by a planar waveguide. Opt Laser Technol 44(7):2286–2291
2. R.C.Jorgenson (1993) Surface plasmon resonance based bulk optic and fiber optic sensors. University of Washington, Washington 40 pp
3. Homola J, Yee S, Gauglitz G (1999) Surface plasmon resonance sensors. ReviewSensors and Actuators B 54:3–15
4. Kretschmann E, Raether H (1968) Radiative decay of non-radiative surface plasmons excited by light. ZNaturforsh 23A:2135–2136

5. Gupta BD, Verma RK (2009) Surface plasmon resonance-based fiber optic sensors: principle, probe designs, and some applications. J Sens 2009(2):12
6. Monzon-Hernandez D, Villatoro J, Talavera D, Luna-Moreno D (2004) Optical-fiber surface-plasmon resonance sensor with multiple resonance peaks. Appl Opt 43:1216
7. Piliarik M, Homola J, Manikova Z, Ctyroky J (2003) Surface plasmon resonance based on a polarization-maintaining optical fiber. Sensors Actuators B Chem 90:236
8. Hautakorpi M, Mattinen M, Ludvigsen H (2008) Surface-plasmon-resonance sensor based on three-hole microstructured optical fiber. Opt Express 16(12):8427–8432
9. Zhao Y, Deng Z-q, Li J (2014) Photonic crystal fiber based surface plasmon resonance chemical sensors. Sensors Actuators B Chem 202:557–567
10. Dash JN, Jha R (2015) On the performance of graphene-based D-shaped photonic crystal fibre biosensor using surface plasmon resonance. Plasmonics 10(5):1123–1131
11. Bing P, Li Z, Yao J (2013) Effects of heterogeneity on the surface plasmon resonance biosensor based on three-hole photonic crystal fiber. Opt Eng 52(5):532–543
12. Akowuah EK, Gorman T, Ademgil H, Haxha S (2012) Numerical analysis of a photonic crystal fiber for biosensing applications. IEEE J Quantum Electron 48(11):1403–1410
13. Bing P, Li Z, Yuan S, Yao J, Lu Y (2015) Surface plasmon resonance biosensor based on large size square-lattice photonic crystal fiber. J Mod Opt 63(8):793–797
14. Hassani A, Skorobogatiy M (2006) Design of the microstructured optical fiber-based surface plasmon resonance sensors with enhanced microfluidics. Opt Express 14(24):11616–11621
15. Hassani A, Skorobogatiy M (2007) Design criteria for microstructured optical fiber based surface plasmon resonance sensors. J Opt Soc Am B 24(6):1423–1429
16. Hassani A, Skorobogatiy M (2009) Photonic crystal fiber-based plasmonic sensors for the detection of bio-layer thickness. Journal of the Optical Society of America B, Optical Physics 26(8):1550–1557
17. Yu X, Zhang Y, Pan SS, Shum P, Yan M, Leviatan Y, Li CM (2010) A selectively coated photonic crystal fiber based surface plasmon resonance sensors. J Opt 12(1):015005–015011
18. Rifat AA et al (2016) A novel photonic crystal fiber biosensor using surface plasmon resonance. Procedia Engineering 140:1–7
19. Liu C, Wang F, Lv J, Sun T, Liu Q, Haiwei M, Chu PK (2015) Design and theoretical analysis of a photonic crystal fiber based on surface plasmon resonance sensing. Journal of Nanophotonics 9: 930501–9305010
20. Shuai BB, Li X, Zhang YZ, Liu DM (2012) A multi-core holey fiber based plasmonic sensor with large detection range and high linearity. Opt Express 20(6):5900–5974
21. Zhang PP, Yao JQ, Cui HX, Lu Y (2013) A surface plasmon resonance sensor based on a multi- core photonic crystal fiber. Opt Lett 35(6):1673–1905
22. Yu X, Zhang S, Zhang Y, Ho HP et al (2010) An efficient approach for investigating surface plasmon resonance in asymmetric optical fibers based on birefringence analysis. Opt Express 18(17):17950–17957
23. Zeng J, Liang D (2006) Application of fiber optic surface plasmon resonance sensor for measuring liquid refractive index. J Intell Mater Syst Struct 17(8–9):787–791
24. Zhou C (2013) Theoretical analysis of double-microfluidic-channels photonic crystal fiber sensor based on silver nanowires. Opt Commun 288:42–46
25. Gao D, Guan CY, Wen YW, Zhong X, Yuan LB (2014) Multi-hole fiber based surface plasmon resonance sensor operated at near-infrared wavelengths. Opt Commun 313(4):94–98
26. Sun B, Chen MY, Zhang YK, Yang JC, Yao JQ, Cui HX (2011) Microstructured-core photonic-crystal fiber for ultra-sensitive refractive index sensing. Opt Express 19(5):4091–4100
27. Town GE, Yuan W, McCosker R, Bang O (2010) Microstructured optical fiber refractive index sensor. Opt Lett 35(6):856–858
28. Erdmanis M, Viegas D, Hautakorpi M, Novotny S, Santos JL, Ludvigsen H (2011) Comprehensive numerical analysis of a surface-plasmon-resonance sensor based on an H-shaped optical fiber. Opt Express 19(15):13980–13988
29. Gauvreau B, Hassani A, Fehri MF, Kabashin A, Shoroobogatiy MA (2007) Photonic bandgap fiber-based surface plasmon resonance sensors. Opt Express 15(18):11413–11426
30. Bing PB, Yao JQ, Lu Y, Li ZY (2012) A surface-plasmon-resonance sensor based on photonic-crystal-fiber with large size microfluidic channels. Optica Applicata XLII 3:493–450
31. Rifat AA, Mahdiraji GA, Chow DM, Shee YG, Ahmed R, Adikan FR (2015) Photonic crystal fiber-based surface plasmon resonance sensor with selective analyte channels and graphene-silver deposited core. Sensors 15(5):11499–11510
32. Otupiri R, Akowuah EK, Haxha S (2015) Multi-channel SPR biosensor based on PCF for multi-analyte sensing applications. Opt Express 23(12):15716–15727